ACS APPLIED MATERIALS & INTERFACES

Research Article

www.acsami.org

Nickel Ferrite Nanoparticles Anchored onto Silica Nanofibers for Designing Magnetic and Flexible Nanofibrous Membranes

Feifei Hong,[†,∥] Chengcheng Yan,[†,§,∥] Yang Si,[†,§] Jianxin He,[‡] Jianyong Yu,[†,§] and Bin Ding*[,†,‡,§]

[†]Key Laboratory of Textile Science & Technology, Ministry of Education, College of Textiles, Donghua University, Shanghai 201620, China

[‡]College of Textiles, Zhongyuan University of Technology, Zhenzhou 450007, China

[§]State Key Laboratory for Modification of Chemical Fibers and Polymer Materials, College of Materials Science and Engineering, Donghua University, Shanghai 201620, China

Supporting Information

ABSTRACT: Many applications proposed for magnetic silica nanofibers require their assembly into a cellular membrane structure. The feature to keep structure stable upon large deformation is crucial for a macroscopic porous material which functions reliably. However, it remains a key issue to realize robust flexibility in two-dimensional (2D) magnetic silica nanofibrous networks. Here, we report that the combination of electrospun silica nanofibers with zein dip-coating can lead to the formation of flexible, magnetic, and hierarchical porous silica nanofibrous membranes (SNM). The 290 nm diameter silica nanofibers act as templates for the uniform anchoring of nickel ferrite nanoparticles (size of 50 nm). Benefiting from the homogeneous and stable nanofiber−nanoparticle composite structure, the resulting magnetic SNM can maintain their structure integrity under repeated bending as high as 180° and can facilely recover. The unique hierarchical structure also provides this new class of silica membrane with integrated properties of ultralow density, high porosity, large surface area, good magnetic responsiveness, robust dye adsorption capacity, and effective emulsion separation performance. Significantly, the synthesis of such fascinating membranes may provide new insight for further application of silica in a self-supporting, structurally adaptive, and 2D membrane form.

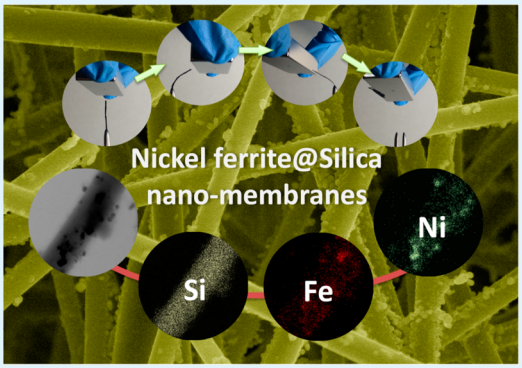

KEYWORDS: *silica nanofibers, electrospinning, flexible membranes, magnetic, nickel ferrite*

1. INTRODUCTION

One-dimensional silica nanofibers have attracted great attention due to the prominent electrical, mechanical, thermal characters, which are promising nanoscale constructing blocks for preparing macroscopic bulk nanofibrous membranes for variety of applications.[1−4] Particularly, introducing magnetic nanoparticles into silica nanofibrous membranes (SNM) is a key issue for fabrication of future materials requiring multifunctional characteristics.[5−8] Up to date, several methods have been invented to fabricate magnetic SNM, such as hydrothermal route, template-assisted process, chemical vapor deposition, and structure-selective synthesis.[9−13] However, previous efforts focused excessively on the morphology and porous structure of SNM, ignoring the brittle feature and poor mechanical properties of the relevant SNM.[14−18] Flexibility that was possessed for membranes with silica-derived sheet or cage nanostructures has not been realized in membranes solely based on silica nanofibers.[3,19] Good mechanical properties (flexibility, tensile strength, and durability) are crucial for the real application of SNM, not only for new generation of flexible electronic devices, including batteries, sensors, supercapacitors, and magnetic actuators, but also for further designing of silica-derived ultralight cellular membranes for bioengineering and environmental remediation.[20−24] Therefore, developing a novel and general method to tackle this important issue is highly desired.

Generally, the performance of magnetic SNM is dictated both by their porous structure and the characters of individual silica nanofibers.[25,26] Alternatively, electrospinning has been shown to be a simple but powerful technique for the preparation of both organic and inorganic functional fibers at the nano- and mesoscale levels. The large specific surface area, high open porosity, good interconnectivity, and fine flexibility make electrospun nanofibers highly attractive as exceptional nanoscale building blocks for constructing mechanical robust magnetic SNM.[27−29] Despite their outstanding potential, only few efforts have been made to use electrospun nanofibers for the preparation of magnetic SNM.[26,30,31] The major problem is that the functional nanoparticles are easy to aggregate in fibrous structure at high concentration, and the resultant membranes

Received: June 27, 2015
Accepted: August 24, 2015
Published: August 24, 2015

DOI: 10.1021/acsami.5b05754
ACS Appl. Mater. Interfaces 2015, 7, 20200−20207

usually become extremely brittle. The problem of aggregation worsens for magnetic nanoparticles and their nanocomposites due to the significant interparticle dipolar forces. This issue has never been systematically addressed before.

Herein, we report a robust method for preparing flexible and magnetic $NiFe_2O_4$@SiO_2 nanofibrous membranes (NiFe@SNM) with a hierarchical porous structure which was composed of $NiFe_2O_4$ nanoparticles ($NiFe_2O_4$ NPs) anchored silica nanofibers. The feature of our methodology is that the $NiFe_2O_4$ NPs are nonagglomerated and firmly anchored onto the surface of silica nanofibers by a facile zein dip-coating method. Benefiting from good nanoparticle−nanofiber bonding and hierarchical porous structure, the NiFe@SNM demonstrates a variety of promising properties including extraordinary flexibility, low density, high porosity, larger surface area, and excellent magnetic responsiveness. We also demonstrate that the NiFe@SNM can effectively adsorb the organic dyes in water and separate the oil/water emulsions.

2. EXPERIMENTAL SECTION

2.1. Materials. Poly(vinyl alcohol) (PVA, Mw = 88000), phosphoric acid (H_3PO_4, 85 wt %), ethanol were provided by Shanghai Chemical Reagents Co., Ltd., China. Tetraethyl otrhosilicate (TEOS) was purchased from Lingfeng Chemical Co., Ltd., China. Ferric chloride ($FeCl_3·6H_2O$), nickel chloride ($NiCl_2·6H_2O$) were purchased from Shanghai Aladdin Chemical Co., China. Zein was provided by Nanjing Duly Biotech Co., Ltd.

2.2. Preparation of SNM. First, 30 g of PVA powders were dissolved in 70 g of pure water at 80 °C with stirring for 10 h. The silica sol was prepared by mixing TEOS, H_3PO_4, and H_2O (molar ratio of 1/0.01/11) with stirring for 8 h at room temperature. Subsequently, 10 g of the resultant PVA solution was mixed with 10 g of the silica sol to obtain a homogeneous solution. Following, the electrospinning was carried on a DXES-3 spinning equipment with an electrostatic voltage of 20 kV and a spinning rate of 1 mL h^{-1}. The relevant temperature was 25 ± 2 °C and the relative humidity was 45 ± 5%. Finally, the composite membranes were calcined at 850 °C with a heating rate of 5 °C min^{-1} in air to remove the PVA component and get SNM.

2.3. Fabrication of NiFe@SNM. The detailed synthesis pathway is schematically shown in Figure 1a. Generally, 50 g of metal salts

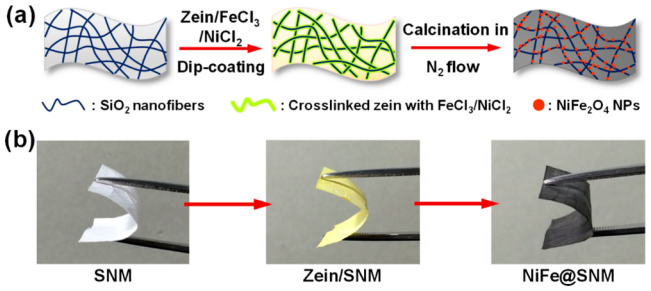

Figure 1. (a) Schematic illustration of the fabriation steps of NiFe@SNM. (b) Optical images of the SNM, zein/SNM, and NiFe@SNM.

solutions with different $FeCl_3$ and $NiCl_2$ concentrations (the molar ratio of Ni:Fe ratio of 1:2) were prepared by adding relevant amount of $FeCl_3·6H_2O$ and $NiCl_2·6H_2O$ to deionized water. Next, 2 g of zein was dissolved in 48 g of ethanol aqueous solution (70 wt %) under stirring. Then, the zein solution was dropwise added to the metal salts solution under stirring, until forming a homogeneous mixed zein sol. Subsequently, the SNM were cut into 2 × 2 cm pieces and dipped in the mixed zein sol for 2 min. After that, the resultant membranes were dried in the vacuum oven at 60 °C, and following treated with microwave with a power of 500 W for 2 min. Thus, the zein layer with embedded $FeCl_3$ and $NiCl_2$ was gradually cross-linked and fixed on the surface of silica nanofibers. It was companied by the color transition from white SNM to yellow zein/SNM at the same time. Finally, the zein/SNM were calcined at 750 °C for 30 min with the heating rate of 5 °C min^{-1} in N_2 flow (the N_2 flow rate was 0.002 m^3 min^{-1}) to obtain black magnetic NiFe@SNM, as shown in Figure 1b. The relevant NiFe@SNM with the metal salt concentration of *x* wt % were denoted as NiFe@SNM-*x*. Detailed information about the zein dip-coating method is presented in the Supporting Information.

2.4. Characterization. Field emission scanning electron microscopy (FE-SEM) images were examined by Hitachi S-4800, Hitachi Ltd., Japan. Scanning transmission electron microscopy (STEM) and energy-dispersive X-ray spectroscopy (EDX) images were measured by using JEM-2100F, JEOL Ltd., Japan. Transmission electron microscopy (TEM) images were measured by using JEM-2100, JEOL Ltd., Japan. Fourier transform infrared spectroscopy (FT-IR) were performed with a Nicolet 8700 FT-IR spectrometer in the range of 4000−400 cm^{-1}. The phase structure was characterized with X-ray diffraction (XRD, D/Max-2550 PC Rigaku Co., Japan). The surface area and porous structure of membranes were characterized by N_2 adsorption−desorption isotherms with a surface area analyzer (ASAP2020, Micromeritics Co., Norcross, GA). Magnetic properties were measured with a vibrating sample magnetometer (VSM, Lake Shore 7304). The dye adsorption properties were measured with a UV−vis spectra (PG2000-Pro, Ideaoptics Technology Ltd., China). The mechanical properties of the membranes were measured on a tensile tester (XQ-1C, Shanghai New Fiber Instrument Co., Ltd., China), and the bending rigidity were measured on a softness tester (RRY-1000, Hangzhou Qingtong & Boke Automation Technology Co., Ltd., China), as demonstrated in Figure S1.

3. RESULTS AND DISCUSSION

3.1. NiFe@SNM Design: Optimizing the Structure and Flexibility. Optimizing the structure design to produce NiFe@SNM with robust flexibility and magnetic properties requires the anchoring of $NiFe_2O_4$ NPs onto silica nanofibers with good homogeneity and stability. As a result, the NiFe@SNM are designed based on three important rules: (1) the electrospun silica nanofibers should assemble into flexible fibrous membranes, (2) the $NiFe_2O_4$ NPs must be nonagglomerated anchoring onto silica nanofibers, (3) the nanofiber−nanoparticle hierarchical structure must be stable without collapsing upon post treatment. The first requirement was satisfied by a stabilizer-free and sol−gel electrospinning method, including the formation of silica sol, the gel-spinning process, and the calcination. To satisfy the other criteria, we used a readily accessible zein dip-coating method to achieve the uniform and well-bonded nanofiber−nanoparticle fibrous networks.

The representative FE-SEM image of pristine SNM presented in Figure 2a indicated a randomly oriented 2D nonwoven membranes with an average fiber diameter of 290 nm and tightly interlacement among fibers. Upon zein dip-coating, the surface of silica fibers was covered by a zein layer (Figure 2b), thus leading to an obvious increase in fiber diameter (406 nm) and cement among adjacent nanofibers. Evidence for the formation of cross-linked zein layer also arose from the FT-IR spectral analysis (Figure 2d), the peaks around 3280 and 1723 cm^{-1} were assigned to the N−H stretching vibration and C═O stretching vibration of amide groups, respectively.[32,33] Moreover, the zein processes the ability to associate with metal ions through the numerous of amino and carboxylic groups, which could readily carry and fix numerous of iron and nickel ions on fiber surface in the dip-coating process.[34,35] After calcination, the zein layer gradually decomposed and the average diameter of fiber reverted back to 309 nm, which was further verified by FE-SEM and FT-IR analysis (Figure 2c,d). Simultaneously, the inner iron and nickel

DOI: 10.1021/acsami.5b05754
ACS Appl. Mater. Interfaces 2015, 7, 20200−20207

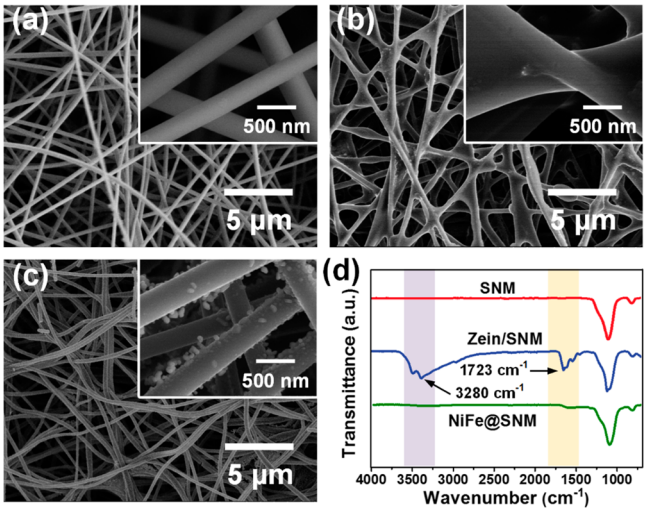

Figure 2. FE-SEM images of (a) SNM, (b) zein/SNM-4, and (c) NiFe@SNM-4. (d) FT-IR spectra of SNM, zein/SNM-4, and NiFe@SNM-4.

ions gradually changed to magnetic $NiFe_2O_4$ NPs via in situ nucleation/growth and were strongly anchored onto the fiber surface.[36,37] In addition, the high magnification FE-SEM images to evidence the surface and morphology changes of SNM and NiFe@SNM were demonstrated in Figure S2.

The introduction of $NiFe_2O_4$ NPs is crucial for creating a functional surface with a hierarchical structure. On the basis of this principle, the hierarchical structure of NiFe@SNM was controlled by changing the concentration of metal salts in zein sols from 0.5 to 8 wt %. As shown in Figure 3a–e, by inclusion

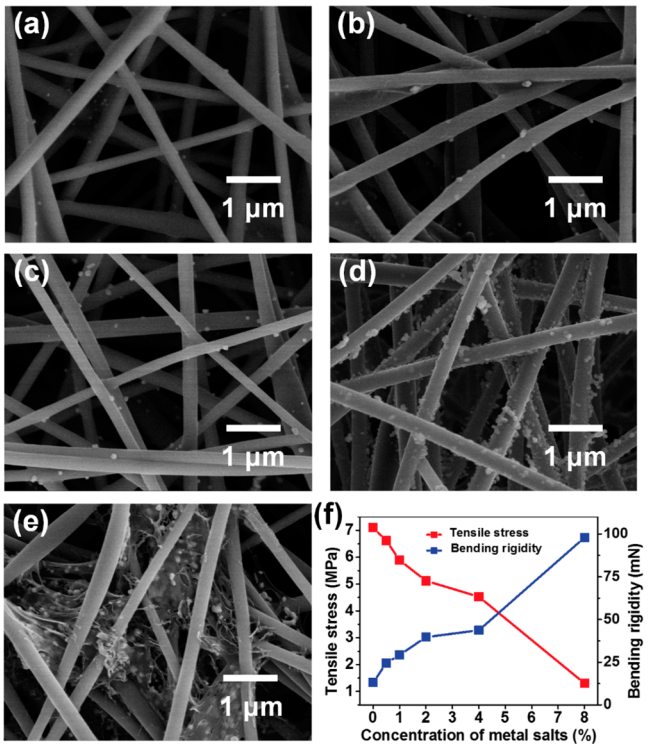

Figure 3. FE-SEM images of (a) NiFe@SNM-0.5, (b) NiFe@SNM-1, (c) NiFe@SNM-2, (d) NiFe@SNM-4, and (e) NiFe@SNM-8. (f) Breaking tensile stress and bending rigidity of various NiFe@SNM with different metal salt contents.

of $NiFe_2O_4$ NPs, the morphologies of resultant membranes were remarkably changed by creating nanoscaled rough structures on the surface of nanofibers. It is clearly showed that the $NiFe_2O_4$ NPs were well-anchored onto the silica fiber surface as metal salt concentration increased from 0.5 to 4 wt %, and a negligible amount of $NiFe_2O_4$ NPs was presented among the voids of nanofibers. As the metal salt content was further increased to 8%, $NiFe_2O_4$ NPs gave rise to aggregation and then filled the voids among fibers,[25,38] which could be attributed to the excessive viscosity of zein sol that impeded the homodispersion of $NiFe_2O_4$ NPs.

Unlike the brittle nature of common ceramic nanofibrous membranes, the NiFe@SNM (taking NiFe@SNM-4 as an example) can bear repeated bending as high as 180° (Figure S3 and Movie S1). It can be seen from Figure S4 that all the tensile stress–strain curves exhibited a nonlinear elastic behavior in the first region (with a robust Young's modulus of about 320 MPa) under a stress load, and then the stress–strain curves exhibited a typical linear increase until breakage. When a first small external load (<1 MPa) is applied, the relevant nonaligned silica nanofibers in membranes were forced to align along the stress direction, resulting in the first nonlinear elastic behavior.[13,15] With continually increasing the tensile stress, the curves showed a typical linear increase until yield, which could be attributed to the slippage of silica nanofibers.[10,15] More interestingly, the amount of $NiFe_2O_4$ NPs in membranes also significantly affected the mechanical properties of relevant membranes. As shown in Figure 3f, the pristine SNM possessed a robust breaking tensile stress of 7.1 MPa and bending rigidity of 13.11 mN. With the increase of metal salt content to 4 wt %, the tensile stress of NiFe@SNM slightly decreased from 6.62 to 4.53 MPa. Further increasing metal salt content to 8 wt % led to a dramatic plunge of stress to 1.30 MPa. The opposite trend of changing the bending rigidity toward increasing metal salt contents could be also observed. This phenomenon was attributed to the filling of voids by a high content of $NiFe_2O_4$ NPs, which restricted the bending and slippage of nanofibers, as demonstrated in the above FE-SEM observation.

3.2. Nanofiber–Nanoparticle Hierarchical Structure.

To provide insight into the nanofiber–nanoparticle hierarchical structure, we performed the STEM and EDX analysis for as-prepared NiFe@SNM (NiFe@SNM-4 was taken as example). Figures 4a–e revealed that Fe and Ni elements were uniformly anchored onto the nanofiber surface, along with Si and O elements. As shown in Figure 4f, the EDX pattern confirmed the molar ratio of Ni and Fe is 1:2, which was consistent with the composition of $NiFe_2O_4$. The calculated content of $NiFe_2O_4$ NPs in the composite membrane was 30.5 wt %, demonstrating that the SNM with high content of magnetic $NiFe_2O_4$ NPs could be easily and scalable fabricated via the proposed approach. Additionally, during the fabrication of STEM specimen, although the NiFe@SNM were treated by high-speed stirring and long-time sonication (30 min), the $NiFe_2O_4$ NPs were still well-anchored onto the silica nanofibers surface, indicating the prominent stability of the nanofiber–nanoparticle hierarchical structure of NiFe@SNM. This firm adhesion effect benefited from the residual carbon on fiber surface, which was derived from the incomplete decomposition of zein during calcination, as shown in the EDX pattern.

As can be seen from the TEM image (Figure 5a), the $NiFe_2O_4$ NPs were homogeneously anchored onto the silica fiber surface, which increased the roughness and surface area of matrix silica fibers. Moreover, the statistic size curve of $NiFe_2O_4$

DOI: 10.1021/acsami.5b05754
ACS Appl. Mater. Interfaces 2015, 7, 20200–20207

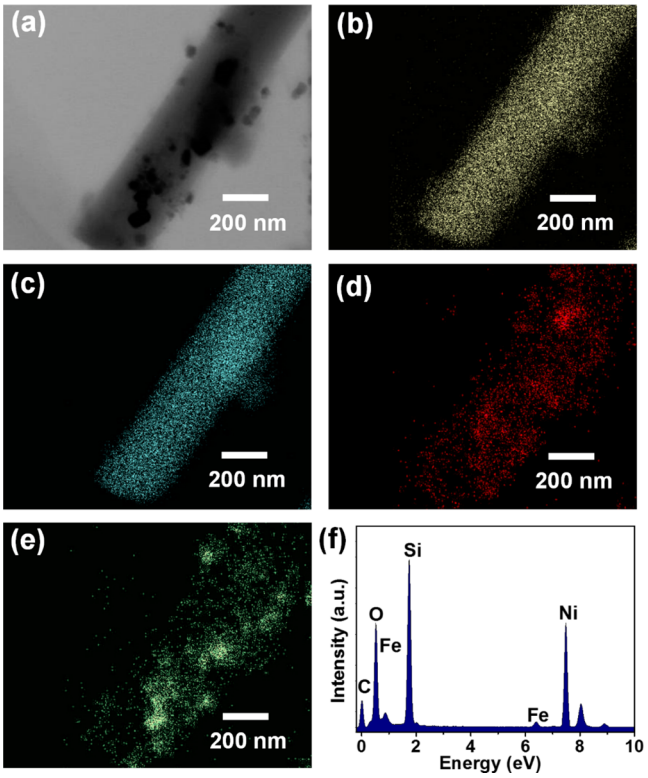

Figure 4. (a) STEM image of the NiFe@SNM-4. STEM with element map images of (b) Si, (c) O, (d) Fe, and (e) Ni. (f) EDX pattern of NiFe@SNM-4.

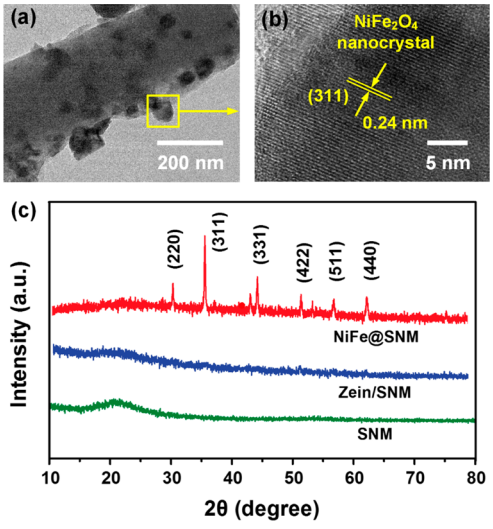

Figure 5. (a) TEM and (b) HRTEM showing the $NiFe_2O_4$ nanocrystals in (311) orientation. (c) XRD patterns of SNM, zein/SNM-4, and NiFe@SNM-4.

NPs presented in Figure S5 revealed a typical polydisperse size ranging from 20 to 80 nm, and an average particle size of 50 nm could be confirmed. The corresponding high-resolution TEM (HRTEM) image (Figure 5b) revealed that the lattice fringe distance deriving from the (311) crystal plane of $NiFe_2O_4$ was 0.24 nm. In combination with the XRD presented in Figure 5c, the relative intensities and positions of diffraction peaks at 2θ values of 30.4° (220), 35.8° (311), 44.6° (331), 51.2° (422), 57.5° (511), and 63.1° (440) matched well with the standard XRD data of the $NiFe_2O_4$ phase (JPPDS No. 10-0325), indicating the crystalline spinel structure of $NiFe_2O_4$ without any additional diffraction of second phases.[37,39] The corresponding crystallite sizes of $NiFe_2O_4$ NPs calculated by Scherrer equation range from 30 to 50 nm, which matched well with the as-characterized TEM observation.

3.3. Quantitatively Porous Structure Analysis. The introduction of magnetic $NiFe_2O_4$ NPs endowed the as-prepared silica membranes with hierarchical architecture and roughness, which dramatically increased the surface area and porosity of nanofibrous membranes. To comprehensively explore the pore structure of resultant membranes, we performed N_2 adsorption−desorption measurement to analysis the BET surface area and pore size distribution (PSD) of the relevant NiFe@SNM samples. As shown in Figure 6a, all the

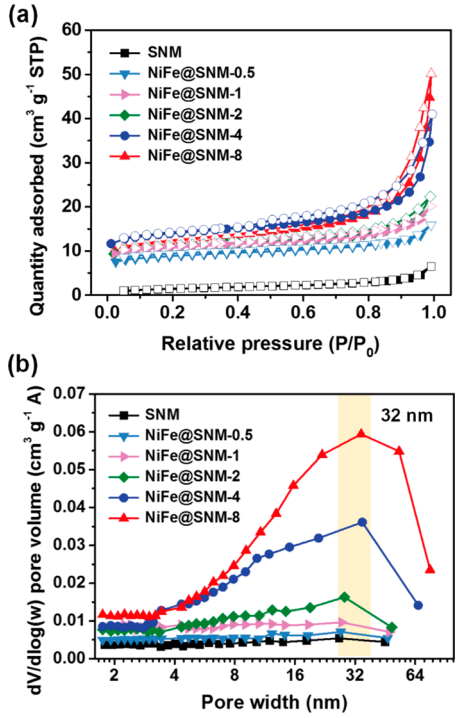

Figure 6. (a) N_2 adsorption−desorption isotherms of SNM, NiFe@SNM-0.5, NiFe@SNM-1, NiFe@SNM-2, NiFe@SNM-4, and NiFe@SNM-8. (b) BJH porous structure analysis of various samples.

isotherm curves of N_2 adsorption−desorption revealed the type IV isotherms according to the IUPAC classification, which included a series of adsorption behaviors including monolayer adsorption, multilayer adsorption and capillary condensation.[40,41] Variations of the above adsorption curves implied an obviously narrow H1 hysteresis loop in the P/P_0 region of 0.4−0.9, indicating the existence of open mesopores in structure. Hence, there was no significant interruption between the capillary evaporation and condensation for N_2 during the adsorption process.[42,43] The detailed BET specific surface area for the NiFe@SNM samples were listed in Table 1. It clearly showed that the BET surface area increased from 5.35 to 45.23 $m^2\ g^{-1}$ with the increasing of the salt contents, which were comparable with previous reported self-stranding silica nanofibers.[44−46]

The quantitative porous structure was further investagted by Barrett−Joyner−Halenda (BJH) method. Figure 6b showed that the BJH PSD curves of all samples presented the polydispersity of pore width ranging from 16 to 64 nm, with

DOI: 10.1021/acsami.5b05754
ACS Appl. Mater. Interfaces 2015, 7, 20200−20207

Table 1. Structure Parameters of Various NiFe@SNM Nanofibrous Membranes with Different Concentrations of Metal Salts

samples	BET surface area (m^2 g^{-1})	BJH pore volume (cm^3 g^{-1})
SNM	5.35	0.009
NiFe@SNM-0.5	28.59	0.015
NiFe@SNM-1	34.62	0.019
NiFe@SNM-2	35.20	0.023
NiFe@SNM-4	40.05	0.051
NiFe@SNM-8	45.23	0.069

a well-developed peak around 32 nm. Moreover, as demonstrated in Figure S6, the pristine SNM exhibited a low BJH pore volume of 0.009 cm^3 g^{-1}, and following the BJH pore volumes showed a great increase with the increasing of $NiFe_2O_4$ NPs content, in which the NiFe@SNM-8 exhibited the maximum pore volume of 0.069 cm^3 g^{-1}. The more than 7 times increasing of porosity indicated the critical role of $NiFe_2O_4$ NPs on controlling the porosity of membranes. Because most of these pores are located at the outside of the fiber rather than inside of the fiber, the composite NiFe@SNM could still keep robust flexibility.

3.4. Magnetic Responsiveness and Application Performance. The representative magnetic hysteresis (M–H) curve of NiFe@SNM (NiFe@SNM-4 was taken as example) shown in Figure 7a demonstrated a nonlinear and reversible

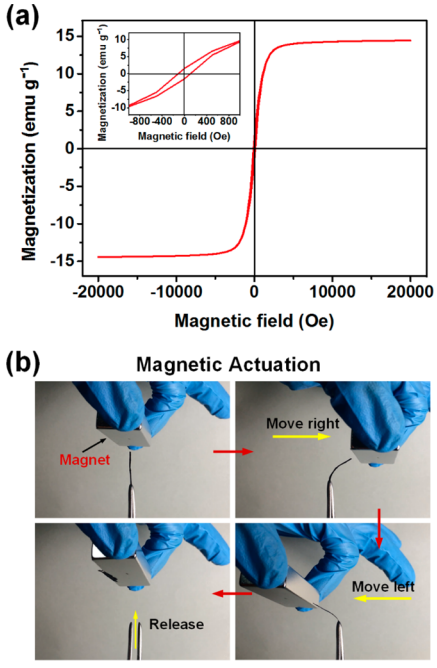

Figure 7. (a) Magnetization curve for the NiFe@SNM-4. (b) Photographs showed the NiFe@SNM-4 membranes could be facilely manipulated by a small magnet.

behavior, which was a typical curve for soft magnetic materials with low remanence, low coercivity, and low loss.[47,48] This robust magnetic property was associated with the fine grain sizes of the embedded $NiFe_2O_4$ NPs demonstrated by the TEM observations. Moreover, as shown in the inset of Figure 7a, a quite small magnetic hysteresis loop (±108 Oe) could be observed after the removal of the magnetic field. Superparamagnetic membranes could be further expected by further decreasing the size of $NiFe_2O_4$ NPs.[47,49] The measured saturation magnetization (M_s) of NiFe@SNM-4 was up to 14.44 emu g^{-1}, which was responsible for the high content of $NiFe_2O_4$ NPs in membrane structure. Considering the relative amount of $NiFe_2O_4$ NPs in membranes (30.5 wt %), it could be analogized that the equivalent M_s of synthesized $NiFe_2O_4$ NPs was 47.26 emu g^{-1}, which was higher than that of previous reported $NiFe_2O_4$ NPs by using protein methods (Table S1).[36,50−52] This value was also quite close to the standard M_s of $NiFe_2O_4$ crystals (50 emu g^{-1}).[36,37] Interestingly, Figure 7b showed that an external magnet could readily actuate the NiFe@SNM-4 sample bending and recovering (Movie S2). Previous reported responsive materials and actuators were mainly liquid ferrogels and hydrogels with magnetic nanoparticles; however, drying of these materials would cause significant brittleness, rendering them impractical applications.[5,53] Therefore, the as-prepared NiFe@SNM with both magnetic property and flexibility might unlock the significant technological perspectives.

Nanostructured materials have the possibility applied as effective adsorbents to remove organic dyes.[54,55] Herein, the NiFe@SNM which included robust porosity and magnetic property were expected for effective adsorption of organic containments in water and fast magnetic separation. We used methylene blue (MB) dye as a model containment to investigate the adsorption performance of as-prepared membranes. In a general experiment, 50 mg of NiFe@SNM-4 was immersed into the test aqueous solution (1×10^{-5} M, 20 mL) with stirring for a designated time, and the test solution was subsequently measured by UV–vis spectra. As the relevant adsorption curves shown in Figure 8a and Figure S7, NiFe@SNM-4 demonstrated promising adsorption ability that it could adsorb 85% of the MB dye for 10 min, and all the dye could be completely adsorbed in 20 min, which was attributed to the enhanced porous structure by $NiFe_2O_4$ modification. This adsorption performance was also comparable with previous

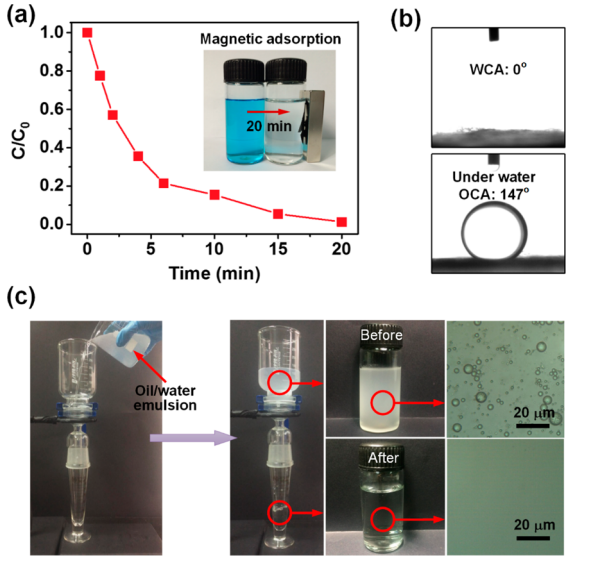

Figure 8. (a) Dye adsorption test of the NiFe@SNM-4 and (inset) graph showing the magnetic responsive of NiFe@SNM-4. (b) Optical profiles of (top) WCA and (bottom) underwater OCA tests on the surface of NiFe@SNM-4. (c) Apparatus showed the facile separation of oil/water emulsion, the right panel showed the optical and microscopic images of pristine emulsions and collected filtrate.

DOI: 10.1021/acsami.5b05754
ACS Appl. Mater. Interfaces 2015, 7, 20200−20207

reported self-stranding silica nanofibers.[56,57] More importantly, the aqueous suspension after adsorption could be purified easily by an external magnet without tedious separation process (Figure 8a, inset) which was of great importance for the treatment of wastewater containing organic pollutants.

We further demonstrated that the NiFe@SNM exhibited robust selective wettability. Benefiting from the high surface energy of the $NiFe_2O_4$ NPs on fiber surface,[58] the NiFe@SNM exhibited superhydrophilicity, with a water contact angle (WCA) of 0°, and robust under water oleophobicity, with an under water−oil contact angle (OCA) of 147° (Figure 8b). Therefore, the oil droplets in emulsions could not pass through the membranes, while water could facilely permeate them. The test surfactant-stabilized (Tween 80) oil-in-water emulsions were prepared by using high-speed stirring and supersonic treatment; thus, a homogeneous emulsion with an average oil droplet size of 5.46 μm could be obtained. As shown in Figure 8c, a circular NiFe@SNM-4 membranes (diameter of 38 mm) were sandwiched between two vertical glass tube. The emulsion was added to the upper tube, the water quickly permeated through the membranes while the oil were retained above, as demonstrated in Movie S3. Optical image analysis revealed that the NiFe@SNM-4 membranes nearly removed all the oil droplets, with no droplets being observed in collected filtrate, demonstrating the high effectiveness for separating oil/water emulsions. Significantly, the NiFe@SNM-4 showed a high separation flux of 3177 ± 214 L m^{-2} h^{-1}, which was 1 order of magnitude higher than that of traditional filtration membrane driven by external pressure.[15,59] In addition, the antifouling performance was performed as displayed in Figure S8. For each cycle, the NiFe@SNM-4 membranes continuously separated a certain amount of emulsion (500 mL) and then the membranes were simply rinsed with ethanol to recover the flux. It can be seen that the flux remained stable with nearly no flux changes after 10 cycles, which could be attributed to the good flexibility and mechanical strength of the membranes during cycle separation. These results indicate an excellent antifouling property of the NiFe@SNM membranes for long-term use.

4. CONCLUSIONS

In conclusion, we have reported a synergistic assembly method for the preparation of flexible, magnetic, and hierarchical porous NiFe@SNM through the combination of sol−gel electrospinning and zein dip-coating methods. The inorganic silica nanofibers were used as templates for the anchoring of $NiFe_2O_4$ NPs with good homogeneity and stability. With their integrated properties of extraordinary flexibility, ultralow density, high porosity, larger surface area, good magnetic responsiveness, robust adsorption capacity, effective emulsion separation, and scalable synthesis all integrated together, we expect the NiFe@SNM will have particularly attractive for numerous applications in a range of fields such as soft electronic devices, medical diagnosis, drug delivery, ferrofluids, magnetic sensing, oil/water separation, and water purification. Furthermore, this work makes it possible to investigate the performances and applications of silica in a self-supporting, structurally adaptive, 2D membrane form. The NiFe@SNM can also incorporate with other functional materials for further design and development of various new silica-derived multifunctional membranes.

■ ASSOCIATED CONTENT

Supporting Information

The Supporting Information is available free of charge on the ACS Publications website at DOI: 10.1021/acsami.5b05754.

Details of mechanical property measurements, bending properties, tensile stress−strain curves, porous structure, UV−vis spectra of MB adsorption, and cycle separation performance. (PDF)
Movie S1 (AVI)
Movie S2 (AVI)
Movie S3 (AVI)

■ AUTHOR INFORMATION

Corresponding Author

*E-mail: binding@dhu.edu.cn.

Author Contributions

∥The manuscript was written through contributions of all authors. All authors have given approval to the final version of the manuscript. These authors contributed equally to this work.

Notes

The authors declare no competing financial interest.

■ ACKNOWLEDGMENTS

This work is supported by the National Natural Science Foundation of China (No. U1232116 and 51322304), the Shanghai Committee of Science and Technology (No. 12JC1400101), the Fundamental Research Funds for the Central Universities, and the "DHU Distinguished Young Professor Program".

■ REFERENCES

(1) Warren, S. C.; Perkins, M. R.; Adams, A. M.; Kamperman, M.; Burns, A. A.; Arora, H.; Herz, E.; Suteewong, T.; Sai, H.; Li, Z. H.; Werner, J.; Song, J. H.; Werner-Zwanziger, U.; Zwanziger, J. W.; Gratzel, M.; DiSalvo, F. J.; Wiesner, U. A Silica Sol-Gel Design Strategy for Nanostructured Metallic Materials. *Nat. Mater.* **2012**, *11*, 460−467.

(2) Gaharwar, A. K.; Mihaila, S. M.; Swami, A.; Patel, A.; Sant, S.; Reis, R. L.; Marques, A. P.; Gomes, M. E.; Khademhosseini, A. Bioactive Silicate Nanoplatelets for Osteogenic Differentiation of Human Mesenchymal Stem Cells. *Adv. Mater.* **2013**, *25*, 3329−3336.

(3) Cai, J.; Liu, S.; Feng, J.; Kimura, S.; Wada, M.; Kuga, S.; Zhang, L. Cellulose-Silica Nanocomposite Aerogels by In Situ Formation of Silica in Cellulose Gel. *Angew. Chem., Int. Ed.* **2012**, *51*, 2076−2079.

(4) Li, Y.; Budamagunta, M. S.; Luo, J.; Xiao, W.; Voss, J. C.; Lam, K. S. Probing of The Assembly Structure and Dynamics within Nanoparticles during Interaction with Blood Proteins. *ACS Nano* **2012**, *6*, 9485−9495.

(5) Barakat, N. A. M.; Khalil, K. A.; Mahmoud, I. H.; Kanjwal, M. A.; Sheikh, F. A.; Kim, H. Y. CoNi Bimetallic Nanofibers by Electrospinning: Nickel-Based Soft Magnetic Material with Improved Magnetic Properties. *J. Phys. Chem. C* **2010**, *114*, 15589−15593.

(6) Olsson, R. T.; Azizi Samir, M. A. S.; Salazar-Alvarez, G.; Belova, L.; Ström, V.; Berglund, L. A.; Ikkala, O.; Nogués, J.; Gedde, U. W. Making Flexible Magnetic Aerogels and Stiff Magnetic Nanopaper Using Cellulose Nanofibrils as Templates. *Nat. Nanotechnol.* **2010**, *5*, 584−588.

(7) Faivre, D. Multifunctional Materials: Dry but Flexible Magnetic Materials. *Nat. Nanotechnol.* **2010**, *5*, 562−563.

(8) Khaing Oo, M. K.; Yang, Y. M.; Hu, Y.; Gomez, M.; Du, H.; Wang, H. J. Gold Nanoparticle-Enhanced and Size-Dependent Generation of Reactive Oxygen Species from Protoporphyrin IX. *ACS Nano* **2012**, *6*, 1939−1947.

DOI: 10.1021/acsami.5b05754
ACS Appl. Mater. Interfaces 2015, 7, 20200−20207

(9) Wang, X. F.; Akhmedov, N. G.; Duan, Y. H.; Luebke, D.; Hopkinson, D.; Li, B. Y. Amino Acid-Functionalized Ionic Liquid Solid Sorbents for Post-Combustion Carbon Capture. *ACS Appl. Mater. Interfaces* **2013**, *5*, 8670−8677.
(10) Okamura, Y.; Kagawa, F.; Mochizuki, M.; Kubota, M.; Seki, S.; Ishiwata, S.; Kawasaki, M.; Onose, Y.; Tokura, Y. Microwave Magnetoelectric Effect via Skyrmion Resonance Modes in A Helimagnetic Multiferroic. *Nat. Commun.* **2013**, *4*, 2391.
(11) Li, B. Y.; Jiang, B. B.; Fauth, D. J.; Gray, M. L.; Pennline, H. W.; Richards, G. A. Innovative Nano-Layered Solid Sorbents for CO_2 Capture. *Chem. Commun.* **2011**, *47*, 1719−1721.
(12) Li, Y. P.; Xiao, W. W.; Xiao, K.; Berti, L.; Luo, J. T.; Tseng, H. P.; Fung, G.; Lam, K. S. Well-Defined, Reversible Boronate Crosslinked Nanocarriers for Targeted Drug Delivery in Response to Acidic pH Values and cis-Diols. *Angew. Chem., Int. Ed.* **2012**, *51*, 2864−2869.
(13) Ding, B.; Wang, M.; Wang, X.; Yu, J.; Sun, G. Electrospun Nanomaterials for Ultrasensitive Sensors. *Mater. Today* **2010**, *13*, 16−27.
(14) Morris, C. A. Silica Sol as A Nanoglue: Flexible Synthesis of Composite Aerogels. *Science* **1999**, *284*, 622−624.
(15) Si, Y.; Fu, Q.; Wang, X.; Zhu, J.; Yu, J.; Sun, G.; Ding, B. Superelastic and Superhydrophobic Nanofiber-Assembled Cellular Aerogels for Effective Separation of Oil/Water Emulsions. *ACS Nano* **2015**, *9*, 3791−3799.
(16) Sai, H.; Xing, L.; Xiang, J.; Cui, L.; Jiao, J.; Zhao, C.; Li, Z.; Li, F.; Zhang, T. Flexible Aerogels with Interpenetrating Network Structure of Bacterial Cellulose−Silica Composite from Sodium Silicate Precursor via Freeze Drying Process. *RSC Adv.* **2014**, *4*, 30453−30461.
(17) Zhong, D.; Yang, Q.; Guo, L.; Dou, S.; Liu, K.; Jiang, L. Fusion of Nacre, Mussel, and Lotus Leaf: Bio-Inspired Graphene Composite Paper with Multifunctional Integration. *Nanoscale* **2013**, *5*, 5758−5764.
(18) Ding, B.; Lin, J.; Wang, X.; Yu, J.; Yang, J.; Cai, Y. Investigation of Silica Nanoparticle Distribution in Nanoporous Polystyrene Fibers. *Soft Matter* **2011**, *7*, 8376−8383.
(19) Sai, H.; Xing, L.; Xiang, J.; Cui, L.; Jiao, J.; Zhao, C.; Li, Z.; Li, F. Flexible Aerogels Based on An Interpenetrating Network of Bacterial Cellulose and Silica by A Non-Supercritical Drying Process. *J. Mater. Chem. A* **2013**, *1*, 7963−7970.
(20) Wang, J.; Cheng, Q.; Lin, L.; Chen, L.; Jiang, L. Understanding The Relationship of Performance with Nanofiller Content in The Biomimetic Layered Nanocomposites. *Nanoscale* **2013**, *5*, 6356−6362.
(21) Lee, M. W.; An, S.; Latthe, S. S.; Lee, C.; Hong, S.; Yoon, S. S. Electrospun Polystyrene Nanofiber Membrane with Superhydrophobicity and Superoleophilicity for Selective Separation of Water and Low Viscous Oil. *ACS Appl. Mater. Interfaces* **2013**, *5*, 10597−10604.
(22) Barakat, N. A.; Kim, B.; Yi, C.; Jo, Y.; Jung, M.-H.; Chu, K. H.; Kim, H. Y. Influence of Cobalt Nanoparticles' Incorporation on The Magnetic Properties of The Nickel Nanofibers: Cobalt-Doped Nickel Nanofibers Prepared by Electrospinning. *J. Phys. Chem. C* **2009**, *113*, 19452−19457.
(23) Park, J. J.; Lee, J. G.; Kim, D. Y.; Hong, J. H.; Kim, J. J.; Hong, S.; Yoon, S. S. Antibacterial and Water Purification Activities of Self-Assembled Honeycomb Structure of Aerosol Deposited Titania Film. *Environ. Sci. Technol.* **2012**, *46*, 12510−12518.
(24) Luo, B.; Xu, S. A.; Luo, A.; Wang, W. R.; Wang, S. L.; Guo, J.; Lin, Y.; Zhao, D. Y.; Wang, C. C. Mesoporous Biocompatible and Acid-Degradable Magnetic Colloidal Nanocrystal Clusters with Sustainable Stability and High Hydrophobic Drug Loading Capacity. *ACS Nano* **2011**, *5*, 1428−1435.
(25) Si, Y.; Yu, J.; Tang, X.; Ge, J.; Ding, B. Ultralight Nanofibre-Assembled Cellular Aerogels with Superelasticity and Multifunctionality. *Nat. Commun.* **2014**, *5*, 5802.
(26) Yuan, J. J.; Zhu, P. X.; Fukazawa, N.; Jin, R. H. Synthesis of Nanofiber-Based Silica Networks Mediated by Organized Poly(ethylene imine): Structure, Properties, and Mechanism. *Adv. Funct. Mater.* **2006**, *16*, 2205−2212.
(27) Greiner, A.; Wendorff, J. H. Electrospinning: A Fascinating Method for The Preparation of Ultrathin Fibers. *Angew. Chem., Int. Ed.* **2007**, *46*, 5670−5703.
(28) Wang, X.; Ding, B.; Sun, G.; Wang, M.; Yu, J. Electro-Spinning/Netting: A Strategy for The Fabrication of Three-Dimensional Polymer Nano-Fiber/Nets. *Prog. Mater. Sci.* **2013**, *58*, 1173−1243.
(29) Si, Y.; Tang, X.; Ge, J.; Yang, S.; El-Newehy, M.; Al-Deyab, S. S.; Yu, J.; Ding, B. In Situ Synthesis of Flexible Magnetic gamma-Fe_2O_3@SiO_2 Nanofibrous Membranes. *Nanoscale* **2014**, *6*, 2102−2105.
(30) Zhu, G. T.; Li, X. S.; Fu, X. M.; Wu, J. Y.; Yuan, B. F.; Feng, Y. Q. Electrospinning-Based Synthesis of Highly Ordered Mesoporous Silica Fiber for Lab-in-Syringe Enrichment of Plasma Peptides. *Chem. Commun.* **2012**, *48*, 9980−9982.
(31) Liu, M.; Song, F.; Shen, X.; Zhu, Y. Effects of Strontium Silicate on Structure and Magnetic Properties of Electrospun Strontium Ferrite Nanofibers. *J. Sol-Gel Sci. Technol.* **2010**, *56*, 39−46.
(32) Khalil, A. A.; Deraz, S. F.; Elrahman, S. A.; El-Fawal, G. Enhancement of Mechanical Properties, Microstructure, and Antimicrobial Activities of Zein Films Cross-Linked Using Succinic Anhydride, Eugenol, and Citric Acid. *Prep. Biochem. Biotechnol.* **2015**, *45*, 551−567.
(33) Dong, F.; Zhang, M.; Tang, W. W.; Wang, Y. Formation and Mechanism of Superhydrophobic/Hydrophobic Surfaces Made from Amphiphiles through Droplet-Mediated Evaporation-Induced Self-Assembly. *J. Phys. Chem. B* **2015**, *119*, 5321−5327.
(34) Ali, S.; Khatri, Z.; Oh, K. W.; Kim, I. S.; Kim, S. H. Zein/Cellulose Acetate Hybrid Nanofibers: Electrospinning and Characterization. *Macromol. Res.* **2014**, *22*, 971−977.
(35) Chen, Y.; Ye, R.; Liu, J. Understanding of Dispersion and Aggregation of Suspensions of Zein Nanoparticles in Aqueous Alcohol Solutions after Thermal Treatment. *Ind. Crops Prod.* **2013**, *50*, 764−770.
(36) Maensiri, S.; Masingboon, C.; Boonchom, B.; Seraphin, S. A Simple Route to Synthesize Nickel Ferrite ($NiFe_2O_4$) Nanoparticles Using Egg White. *Scr. Mater.* **2007**, *56*, 797−800.
(37) Li, L. P.; Li, G. S.; Smith, R. L.; Inomata, H. Microstructural Evolution and Magnetic Properties of $NiFe_2O_4$ Nanocrystals Dispersed in Amorphous Silica. *Chem. Mater.* **2000**, *12*, 3705−3714.
(38) Sinha-Ray, S.; Lee, M. W.; Sinha-Ray, S.; An, S.; Pourdeyhimi, B.; Yoon, S. S.; Yarin, A. L. Supersonic Nanoblowing: A New Ultra-Stiff Phase of Nylon 6 in 20−50 nm Confinement. *J. Mater. Chem. C* **2013**, *1*, 3491−3498.
(39) Zhang, J.; Fu, J.; Tan, G.; Li, F.; Luo, C.; Zhao, J.; Xie, E.; Xue, D.; Zhang, H.; Mellors, N. J.; Peng, Y. Nanoscale Characterization and Magnetic Reversal Mechanism Investigation of Electrospun $NiFe_2O_4$ Multi-Particle-Chain Nanofibres. *Nanoscale* **2012**, *4*, 2754−2759.
(40) Si, Y.; Ren, T.; Li, Y.; Ding, B.; Yu, J. Fabrication of Magnetic Polybenzoxazine-Based Carbon Nanofibers with Fe_3O_4 Inclusions with A Hierarchical Porous Structure for Water Treatment. *Carbon* **2012**, *50*, 5176−5185.
(41) Saud, P. S.; Pant, B.; Park, M.; Chae, S.; Park, S.; Ei-Newehy, M.; Al-Deyab, S. S.; Kim, H. Preparation and Photocatalytic Activity of Fly Ash Incorporated TiO_2 Nanofibers for Effective Removal of Organic Pollutants. *Ceram. Int.* **2015**, *41*, 1771−1777.
(42) Si, Y.; Ren, T.; Ding, B.; Yu, J.; Sun, G. Synthesis of Mesoporous Magnetic Fe_3O_4@Carbon Nanofibers Utilizing In Situ Polymerized Polybenzoxazine for Water Purification. *J. Mater. Chem.* **2012**, *22*, 4619−4622.
(43) Wang, X. F.; Akhmedov, N. G.; Duan, Y. H.; Luebke, D.; Li, B. Y. Immobilization of Amino Acid Ionic Liquids into Nanoporous Microspheres as Robust Sorbents for CO_2 Capture. *J. Mater. Chem. A* **2013**, *1*, 2978−2982.
(44) Wen, S.; Liu, L.; Zhang, L.; Chen, Q.; Zhang, L.; Fong, H. Hierarchical Electrospun SiO_2 Nanofibers Containing SiO_2 Nanoparticles with Controllable Surface-Roughness and/or Porosity. *Mater. Lett.* **2010**, *64*, 1517−1520.
(45) Newsome, T. E.; Olesik, S. V. Electrospinning Silica/Polyvinylpyrrolidone Composite Nanofibers. *J. Appl. Polym. Sci.* **2014**, *131*, 40966.

DOI: 10.1021/acsami.5b05754
ACS Appl. Mater. Interfaces 2015, 7, 20200−20207

(46) Iimura, K.; Oi, T.; Suzuki, M.; Hirota, M. Preparation of Silica Fibers and Non-woven Cloth by Electrospinning. *Adv. Powder Technol.* **2010**, *21*, 64−68.
(47) Zhong, H.; Xiao, X.; Zheng, S.; Zhang, W.; Ding, M.; Jiang, H.; Huang, L.; Kang, J. Mass Spectrometric Analysis of Mono- and Multi-Phosphopeptides by Selective Binding with $NiZnFe_2O_4$ Magnetic Nanoparticles. *Nat. Commun.* **2013**, *4*, 1656.
(48) Kong, B.; Tang, J.; Wu, Z.; Wei, J.; Wu, H.; Wang, Y.; Zheng, G.; Zhao, D. Ultralight Mesoporous Magnetic Frameworks by Interfacial Assembly of Prussian Blue Nanocubes. *Angew. Chem., Int. Ed.* **2014**, *53*, 2888−2892.
(49) Liu, Y.; Zhang, X.; Xia, Y.; Yang, H. Magnetic-Field-Assisted Electrospinning of Aligned Straight and Wavy Polymeric Nanofibers. *Adv. Mater.* **2010**, *22*, 2454−2457.
(50) Gul, I. H.; Ahmed, W.; Maqsood, A. Electrical and Magnetic Characterization of Nanocrystalline Ni−Zn Ferrite Synthesis by Co-Precipitation Route. *J. Magn. Magn. Mater.* **2008**, *320*, 270−275.
(51) Al Angari, Y. M. Magnetic Properties of La-Substituted $NiFe_2O_4$ via Egg-White Precursor Route. *J. Magn. Magn. Mater.* **2011**, *323*, 1835−1839.
(52) Zhu, H. W.; Zhang, C. P. The Preparation of $NiFe_2O_4$ Composite Nanoparticles and Spectral Properties. *Spectrosc. Spect. Anal.* **2004**, *24*, 25−28.
(53) Wang, X.; Ding, B.; Yu, J.; Wang, M. Engineering Biomimetic Superhydrophobic Surfaces of Electrospun Nanomaterials. *Nano Today* **2011**, *6*, 510−530.
(54) Ren, T.; Si, Y.; Yang, J.; Ding, B.; Yang, X.; Hong, F.; Yu, J. Polyacrylonitrile/Polybenzoxazine-Based Fe_3O_4@Carbon Nanofibers: Hierarchical Porous Structure and Magnetic Adsorption Property. *J. Mater. Chem.* **2012**, *22*, 15919−15927.
(55) Chen, M.; Zhang, L.; Duan, S.; Jing, S.; Jiang, H.; Luo, M.; Li, C. Highly Conductive and Flexible Polymer Composites with Improved Mechanical and Electromagnetic Interference Shielding Performances. *Nanoscale* **2014**, *6*, 3796−3803.
(56) Wang, X.; Fan, H.; Ren, P.; Yu, H.; Li, J. A Simple Route to Disperse Silver Nanoparticles on the Surfaces of Silica Nanofibers with Excellent Photocatalytic Properties. *Mater. Res. Bull.* **2012**, *47*, 1734−1739.
(57) Wang, R.; Guo, J.; Chen, D.; Miao, Y.; Pan, J.; Tjiu, W.; Liu, T. "Tube Brush" Like ZnO/SiO_2 Hybrid to Construct a Flexible Membrane with Enhanced Photocatalytic Properties and Recycling Ability. *J. Mater. Chem.* **2011**, *21*, 19375−19380.
(58) Zhang, F.; Zhang, W. B.; Shi, Z.; Wang, D.; Jin, J.; Jiang, L. Nanowire-Haired Inorganic Membranes with Superhydrophilicity and Underwater Ultralow Adhesive Superoleophobicity for High-Efficiency Oil/Water Separation. *Adv. Mater.* **2013**, *25*, 4192−4198.
(59) Kota, A. K.; Kwon, G.; Choi, W.; Mabry, J. M.; Tuteja, A. Hygro-Responsive Membranes for Effective Oil−Water Separation. *Nat. Commun.* **2012**, *3*, 1025.

DOI: 10.1021/acsami.5b05754
ACS Appl. Mater. Interfaces 2015, 7, 20200−20207